

Blood pressure and blood flow variation during postural change from sitting to standing: model development and validation

Mette S. Olufsen, Johnny T. Ottesen, Hien T. Tran, Laura M. Ellwein, Lewis A. Lipsitz and Vera Novak

J Appl Physiol 99:1523-1537, 2005. First published 28 April 2005; doi:10.1152/jappphysiol.00177.2005

You might find this additional info useful...

This article cites 26 articles, 11 of which can be accessed free at:

</content/99/4/1523.full.html#ref-list-1>

This article has been cited by 8 other HighWire hosted articles, the first 5 are:

A new hemodynamic model for the study of cerebral venous outflow

G. Gadda, A. Taibi, F. Sisini, M. Gambaccini, P. Zamboni and M. Ursino

Am J Physiol Heart Circ Physiol, February 1, 2015; 308 (3): H217-H231.

[\[Abstract\]](#) [\[Full Text\]](#) [\[PDF\]](#)

Hemodynamic performance of the Fontan circulation compared with a normal biventricular circulation: a computational model study

Fuyou Liang, Hideaki Senzaki, Clara Kurishima, Koichi Sughimoto, Ryo Inuzuka and Hao Liu

Am J Physiol Heart Circ Physiol, October 1, 2014; 307 (7): H1056-H1072.

[\[Abstract\]](#) [\[Full Text\]](#) [\[PDF\]](#)

A Sonographic Quantitative Cutoff Value of Cerebral Venous Outflow in Neurologic Diseases: A Blinded Study of 115 Subjects

L. Monti, E. Menci, P. Piu, S. Leonini, U. Arrigucci, M. Bellini, A. Zandonella, P. Galluzzi and A. Casasco

AJNR Am J Neuroradiol, July, 2014; 35 (7): 1381-1386.

[\[Abstract\]](#) [\[Full Text\]](#) [\[PDF\]](#)

Initial orthostatic hypotension and cerebral blood flow regulation: effect of α_1 -adrenoreceptor activity

Nia C. S. Lewis, Philip N. Ainslie, Greg Atkinson, Helen Jones, Emily J. M. Grant and Samuel J. E. Lucas

Am J Physiol Regul Integr Comp Physiol, January 15, 2013; 304 (2): R147-R154.

[\[Abstract\]](#) [\[Full Text\]](#) [\[PDF\]](#)

Bilateral Transit Time Assessment of Upper and Lower Limbs as a Surrogate Ankle Brachial Index Marker

Jong Yong Abdiel Foo

ANGIOLOGY 2008; 59 (3): 283-289.

[\[Abstract\]](#) [\[PDF\]](#)

Updated information and services including high resolution figures, can be found at:

</content/99/4/1523.full.html>

Additional material and information about *Journal of Applied Physiology* can be found at:

<http://www.the-aps.org/publications/jappl>

This information is current as of April 9, 2015.

Blood pressure and blood flow variation during postural change from sitting to standing: model development and validation

Mette S. Olufsen,¹ Johnny T. Ottesen,² Hien T. Tran,¹
Laura M. Ellwein,¹ Lewis A. Lipsitz,^{3,4} and Vera Novak⁴

¹Department of Mathematics, North Carolina State University, Raleigh, North Carolina; ²Department of Mathematics and Physics, Roskilde University, Roskilde, Denmark; and ³Hebrew SeniorLife, Research and Training Institute, and ⁴Division of Gerontology, Beth Israel Deaconess Medical Center and Harvard Medical School, Boston, Massachusetts

Submitted 14 February 2005; accepted in final form 26 April 2005

Olufsen, Mette S., Johnny T. Ottesen, Hien T. Tran, Laura M. Ellwein, Lewis A. Lipsitz, and Vera Novak. Blood pressure and blood flow variation during postural change from sitting to standing: model development and validation. *J Appl Physiol* 99: 1523–1537, 2005. First published April 28, 2005; doi:10.1152/jappphysiol.00177.2005.—Short-term cardiovascular responses to postural change from sitting to standing involve complex interactions between the autonomic nervous system, which regulates blood pressure, and cerebral autoregulation, which maintains cerebral perfusion. We present a mathematical model that can predict dynamic changes in beat-to-beat arterial blood pressure and middle cerebral artery blood flow velocity during postural change from sitting to standing. Our cardiovascular model utilizes 11 compartments to describe blood pressure, blood flow, compliance, and resistance in the heart and systemic circulation. To include dynamics due to the pulsatile nature of blood pressure and blood flow, resistances in the large systemic arteries are modeled using nonlinear functions of pressure. A physiologically based submodel is used to describe effects of gravity on venous blood pooling during postural change. Two types of control mechanisms are included: 1) autonomic regulation mediated by sympathetic and parasympathetic responses, which affect heart rate, cardiac contractility, resistance, and compliance, and 2) autoregulation mediated by responses to local changes in myogenic tone, metabolic demand, and CO₂ concentration, which affect cerebrovascular resistance. Finally, we formulate an inverse least-squares problem to estimate parameters and demonstrate that our mathematical model is in agreement with physiological data from a young subject during postural change from sitting to standing.

cardiovascular system; mathematical modeling; cerebral blood flow; gravitational effect; autonomic regulation; cerebral autoregulation

ORTHOSTATIC INTOLERANCE DISORDERS, which are common in every age, are difficult to diagnose and treat. Typically, these disorders, with clinical manifestations including dizziness, syncope, orthostatic hypotension, falls, and cognitive decline, are a result of several biological mechanisms. To develop better strategies to treat and diagnose orthostatic intolerance, it is important to understand the underlying mechanisms leading to these disorders. One of the main mechanisms involved is the short-term cardiovascular regulation of blood flow to the brain, which includes autonomic regulation and cerebral autoregulation. The overall goal of this work is to develop a mathematical model that can predict dynamics in observed cerebral blood flow and peripheral blood pressure data and propose mechanisms that can explain the interaction between autonomic regulation and cerebral autoregulation. To this end, we have

developed a mathematical model that can predict these two regulatory mechanisms. To validate the model, we compare model predictions with measurements of arterial finger blood pressure and middle cerebral artery blood flow velocity of a young subject.

On the transition from sitting in a chair to standing, blood is pooled in the lower extremities as a result of gravitational forces. Venous return is reduced, which leads to a decrease in cardiac stroke volume, a decline in arterial blood pressure, and an immediate decrease in blood flow to the brain. The reduction in arterial blood pressure unloads the baroreceptors located in the carotid and aortic walls, which leads to parasympathetic withdrawal and sympathetic activation through baroreflex-mediated autonomic regulation. Parasympathetic withdrawal induces fast (within 1–2 cardiac cycles) increases in heart rate, whereas sympathetic activation yields a slower (within 6–8 cardiac cycles) increase in vascular resistance, vascular tone, and cardiac contractility and a further increase in heart rate (4, 7, 37). Simultaneously, cerebral autoregulation, mediated by changes in CO₂, myogenic tone, and metabolic demand, leads to vasodilation of the cerebral arterioles (2, 18, 34, 38).

Our mathematical model includes two submodels: 1) a cardiovascular model that can predict blood pressure and blood flow velocity during sitting and 2) a control model that can predict autonomic and cerebral regulatory mechanisms during the postural change from sitting to standing. Both submodels are based on the same closed-loop model with 11 compartments that represent the heart and systemic circulation. Our previous work (27, 29) also used compartmental models to describe the dynamics of the cardiovascular system. One (27) used an open-loop (3-element windkessel) model to analyze dynamics of cardiovascular control. This model used arterial blood pressure measured in the finger as an input to predict model parameters that describe dynamics of cerebral vascular regulation for young subjects. These parameters were obtained by minimizing the error between computed and measured middle cerebral artery blood flow velocity. Consequently, no equations were used to describe possible mechanisms of the underlying regulation. To further advance this study, we recently developed a seven-compartment closed-loop model (29) that can predict the dynamics observed in the data. This model did not rely on an external input; rather, it included a submodel that describes the pumping of the left ventricle. In addition, the seven-compartment model included simple equations that de-

Address for reprint requests and other correspondence: M. S. Olufsen, Dept. of Mathematics, North Carolina State Univ., Raleigh, NC 27695 (E-mail: msolufse@math.ncsu.edu).

The costs of publication of this article were defrayed in part by the payment of page charges. The article must therefore be hereby marked “advertisement” in accordance with 18 U.S.C. Section 1734 solely to indicate this fact.

scribe the short-term regulation. This model was able to accurately predict dynamics of cerebral blood flow velocity and arterial blood pressure during sitting ($t < 60$ s) and standing ($t > 80$ s), as well as the mean values during the transition from sitting to standing ($60 < t < 80$ s), but it was not able to predict detailed dynamics during the transition from sitting to standing. Furthermore, we were not able to achieve adequate filling of the left ventricle. To obtain a more accurate model, we developed the 11-compartment model, which overcomes limitations of the 7-compartment model by 1) predicting resistances as nonlinear functions of pressure, 2) adding essential compartments, 3) devising an empirical model of autoregulation, and 4) including a new physiological model describing pooling of blood in the lower extremities due to effects of gravity.

A large body of work that describes cardiovascular control modeling (9–11, 30, 44) is based on predictions of mean values for arterial blood pressure and cerebral blood flow velocity. Consequently, these models cannot predict the pulsatile dynamics of the cardiovascular system. These models use optimal control to minimize the deviation between some observed quantity (e.g., arterial blood pressure) and a given set point. Although this strategy can provide good parameter estimates, optimal control models do not describe the underlying physiological mechanisms. Other modeling strategies have been proposed by Melchior et al. (19, 20) and Heldt et al. (8), who devised pulsatile models that include pulsatility, autonomic regulation, and effects of gravity. The latter was done by changing the reference pressure outside the compartments. However, these models do not include effects of autoregulation. One way to model the effect of autoregulation is to let the cerebrovascular resistance be a function of time, as suggested by Ursino and Lodi (39). However, this work does not include the effects of autonomic regulation. A second group of models described parts of the control system without validation against experimental data (5, 19–21, 31, 32, 35, 40–43). These models used a closed-loop compartmental description of the cardiovascular system combined with physiological descriptions of the control. Although these models can provide qualitative analysis of the system, they cannot be used for quantitative comparisons with data. Furthermore, most of the models in the second group describe the effects of autonomic regulation without including the effects of cerebral autoregulation. In contrast, our model includes autonomic and cerebrovascular regulations and provides quantitative comparisons with physiological data.

Glossary

A	Cross-sectional area
a	Aorta
ac	Cerebral arteries (in the brain)
acp	Peripheral cerebral arteries
af	Finger arteries
afp	Peripheral finger arteries
al	Arteries in the lower body
alp	Peripheral arteries in the lower body
au	Arteries in the upper body
aup	Peripheral arteries in the upper body
av	Aortic valve
C	Compliance

c	Contractility
fact	Constant factor (area of vessel)
g	Gravitational acceleration
H	Heart rate
h	Height
k	Constant (steepness of sigmoid)
L	Inertance
l	Length
la	Left atrium
lv	Left ventricle
M	Maximum
m	Minimum
mv	Mitral valve
p	Blood pressure
p_{in}	Pressure at inlet
p_{out}	Pressure at outlet
p_p	Peak value of activation
q	Volumetric flow rate
R	Resistance to flow
r	Radius
T	Duration of the cardiac cycle
t_p	Peak value of contraction
V	Stressed volume
v	Velocity
v	Vena cava
vc	Cerebral veins
vl	Veins in the lower body
V_{stroke}	Stroke volume
vu	Veins in the trunk and upper body
η	Viscosity
ν	Steepness
ρ	Density of fluid
τ	Time constant

MODELING BLOOD PRESSURE AND BLOOD FLOW VELOCITY

Compartmental model for the cardiovascular system. Our cardiovascular model is based on an 11-compartment closed-loop model. The model is designed to predict blood pressure and volumetric blood flow in the left atrium, left ventricle, aorta, vena cava, arteries, and veins in the upper body, lower body, and head, as well as arteries in the finger (Fig. 1). Each compartment represents all vessels in areas of similar pressure. Hence, in its simplest form, the systemic circuit could consist of one arterial (high-pressure) and one venous (low-pressure) compartment. In our model, we include five arterial compartments and four venous compartments.

The 11 compartments depicted in Fig. 1 are chosen to ensure that the level of detail in the model is adequate to describe the complex dynamics observed in the data and, at the same time, is not too complex to be solved computationally. Four compartments that represent the upper body and the legs are included to model venous pooling of blood and sympathetic contraction of the vascular bed. Two compartments that represent the brain are included to model effects of cerebral autoregulation and to enable model validation against cerebral arterial blood flow velocity measurements. One compartment that represents the finger is included to enable model validation against arterial blood pressure measured in the finger. To determine cardiac output and venous return, two compartments

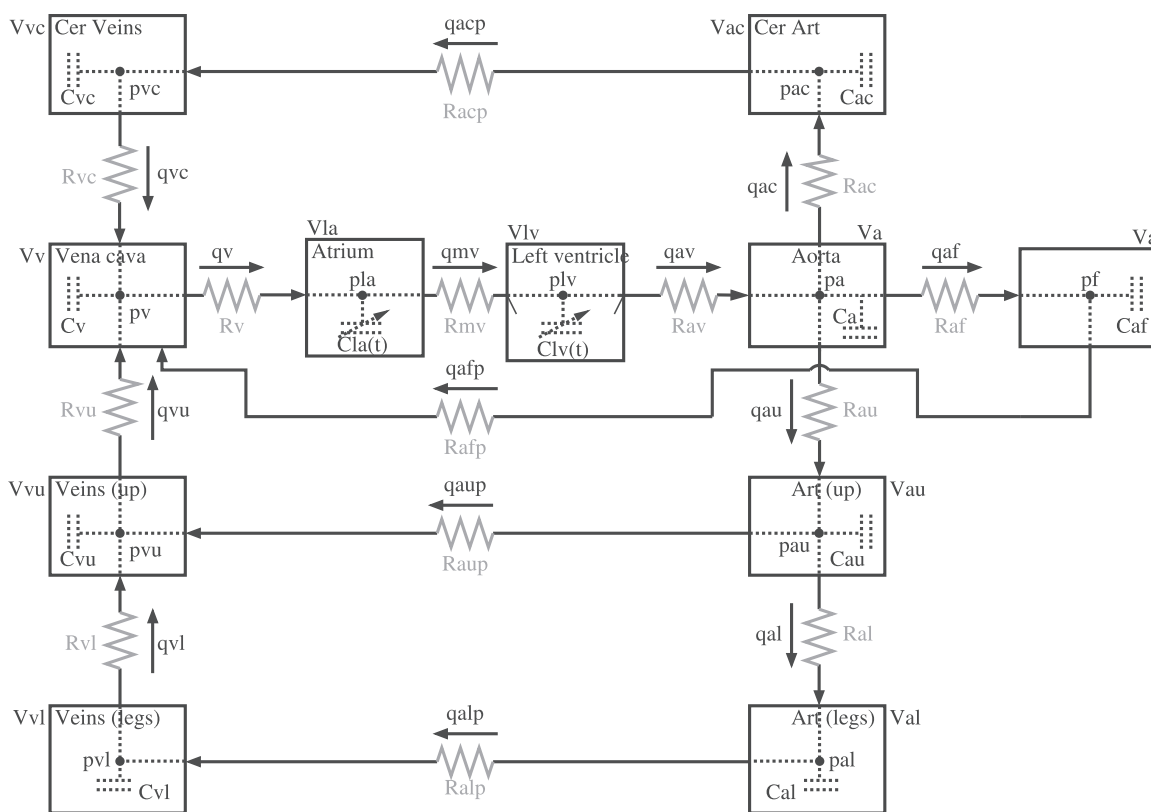


Fig. 1. Compartmental model of systemic circulation. The model contains 11 compartments: 5 represent systemic arteries (brain, upper body, lower body, aorta, and finger), 4 represent systemic veins (brain, upper body, lower body, and vena cava), and 2 represent left atrium and left ventricle. Because the pulmonary system is not included, systemic veins are directly attached to the left ventricle. Each compartment includes a capacitor to represent compliant volume of arteries or veins. All compartments are separated by resistors representing resistance of the vessels. Compartment representing the left ventricle has 2 valves (aortic and mitral). Following terminology from electrical circuit theory, flow between compartments is equivalent to electrical current, and pressure inside each compartment is analogous to voltage. Resistors (R , $\text{mmHg} \cdot \text{s} \cdot \text{cm}^{-3}$) are marked with zigzag lines, capacitors (C , cm^3/mmHg) with dashed parallel lines inside the compartments, and aortic and mitral valves with short lines inside the compartment that represents the left ventricle. Cer, cerebral; see *Glossary* for other abbreviations.

are included to represent the aorta and vena cava. Finally, to obtain a closed-loop model, it is necessary to include a source (i.e., the heart) that pumps blood through the system. Consequently, two compartments are included to represent the left atrium and left ventricle. Our previous work (29) included only the left ventricle; without an atrium, it is not possible to achieve adequate filling of the heart.

The major system not included in our model is the pulmonary circulation. Addition of compartments that represent the pulmonary circulation would require more parameters, which would increase the computational complexity. Instead, the pulmonary circulation is represented as a resistance between the vena cava and the left atrium.

To study dynamics of postural change from sitting to standing, it is not important to know how blood is distributed among various inner organs. Hence, the upper body is simply represented by an arterial and a venous compartment. Each compartment is represented by a compliance element (inverse elasticity) and is separated by resistance to flow. The design of the systemic circulation with arteries and veins separated by capillaries provides some resistance and inertia to the volumetric flow rate. In our model, we include effects of resistance between compartments but neglect effects due to inertia. The major resistance to flow is located in peripheral regions between compartments that represent arteries and veins. Com-

partments that represent large conduit vessels are also separated by resistances that represent the overall resistance of the compartment. Resistances between conduit vessels are very small compared with peripheral resistances.

The description of blood pressure and volumetric flow in a system consisting of compliant compartments (capacitors) and resistors is equivalent to that of an electrical circuit (Fig. 1), where blood pressure plays the role of voltage and volumetric flow rate plays the role of current. To compare our model with data, we assume that the diameter of the middle cerebral artery remains constant, such that blood flow velocity can be obtained by scaling volumetric blood flow by a constant factor that represents the area of the vessel. Recent measurements of middle cerebral artery diameter by magnetic resonance imaging combined with transcranial Doppler assessment of cerebral blood flow velocity have demonstrated that the middle cerebral artery diameter does not change, despite large changes in cerebral blood flow velocity elicited by stimuli such as lower body negative pressure and CO_2 changes (36).

To predict blood pressure and blood flow within and between the compartments, we base our model on volume conservation laws (41). Blood pressure and volumetric blood flow can be found by computing the volume and change in volume for each compartment. The equations that represent the arterial and venous compartments are similar. For each of these com-

partments, the stressed volume $V = Cp$ (cm^3 , volume pumped out during 1 cardiac cycle), where C (cm^3/mmHg) is compliance and p (mmHg) is blood pressure. The cardiac output (CO) from the heart is given by $\text{CO} = HV_{\text{stroke}}$ (cm^3/s), where H (beats/s) is heart rate and V_{stroke} (cm^3/beat) is stroke volume. For each compartment, the net change of volume is given by

$$\frac{dV}{dt} = q_{in} - q_{out}, \quad q = \frac{P_{in} - P_{out}}{R} \quad (1)$$

where q (cm^3/s) is determined analogously to Kirchhoff's current law and R is the resistance to flow. Several compartments have more than one inflow or outflow. For example, the compartment that represents the aorta has three outflows ($q_{out} = q_{af} + q_{au} + q_{ac}$), whereas the compartment that represents the vena cava has three inflows ($q_{in} = q_{afp} + q_{vu} + q_{vc}$; Fig. 1).

To model the left ventricle as a pump, the position of the mitral and aortic valves must be included. During diastole, the mitral valve is open, while the aortic valve is closed, allowing blood to enter the left ventricle. Then isometric contraction begins, increasing the ventricular pressure. Once the ventricular pressure exceeds the aortic pressure, the aortic valve opens, propelling the pulse wave through the vascular system. For healthy young people, both valves cannot be open simultaneously. To incorporate the state of the valves, we have modeled the resistances (R_{av} and R_{mv} ; Fig. 1) as follows

$$R_v = \min(R_v + e^{-10(p_{in} - p_{out})}, 5,000)$$

where v represents mitral and aortic valves. This equation results in a large resistance (and no flow) while the valve is closed and a small resistance (and normal flow) while the valve is open. The minimum (min) value is introduced to avoid numerical problems due to large numbers.

A system of differential equations is obtained by differentiating the volume equation $V = Cp$ and inserting Eq. 1

$$\frac{dV}{dt} = C \frac{dp}{dt} + p \frac{dC}{dt} = q_{in} - q_{out} \quad (2)$$

The circuit in Fig. 1 gives rise to a total of nine differential equations in dp/dt , one for each of the arterial and venous compartments. For the two compartments that represent the atrium and the ventricle, differential equations are kept as dV/dt . For these two compartments, blood pressure is computed explicitly as a function of volume (see *Ventricular and atrial contraction*; for a complete list of equations, see the APPENDIX).

Ventricular and atrial contraction. Atrial and ventricular contraction leads to an increase in blood pressure from the low values observed in the venous system to the high values observed in the arterial system. Our model is based on the work by Ottesen and coworkers (6, 33), which predicts atrial (p_{la}) and ventricular (p_{lv}) pressure as a function volume and cardiac activation of the form

$$p = a[V(t) - b]^2 + [c(t)V(t) - d]g(t) \quad p = p_{la}, p_{lv} \quad (3)$$

The parameter a (mmHg/cm^3) is related to elastance during relaxation, b (cm^3) represents volume at zero diastolic pressure, $c(t)$ (mmHg/cm^3) represents contractility, and d (mmHg)

is related to the volume-dependent and volume-independent components of developed pressure.

The activation function $g(t)$, which is defined over the length of one cardiac cycle, is described by a polynomial of degree (n, m) : $g(t) = f(t)/f(t_p)$ with

$$f(\tilde{t}) = \begin{cases} p_p \frac{\tilde{t}^n (\beta - \tilde{t})^m}{n^n m^m \left[\frac{\beta}{m+n} \right]^{m+n}}, & 0 \leq \tilde{t} \leq \beta \\ 0 & \beta < \tilde{t} \leq T \end{cases} \quad (4)$$

where T (s) is the duration of the cardiac cycle [$\tilde{t} = \text{mod}(t; T)$, s], $\beta(H)$ (s) denotes the onset of relaxation, $H = 1/T$ (1/s) is heart rate, n and m characterize the contraction and relaxation phases, and p_p is the peak value of the activation. The ability to vary heart rate is included in the isovolumic pressure equation (Eq. 3) by scaling time and peak values of the activation function f . The time for peak value of the contraction [t_p (s)] is scaled by introducing a sigmoidal function, which depends on the heart rate (H), of the form

$$t_p = t_m + \frac{\theta^v}{H^v + \theta^v} (t_M - t_m) \quad (5)$$

where θ represents the median, v represents steepness, and t_m (s) and t_M (s) denote the minimum and maximum values, respectively. The peak ventricular pressure [p_p (mmHg)] is scaled similarly using a sigmoidal function of the form

$$p_p = p_m + \frac{H^\eta}{H^\eta + \varphi^\eta} (p_M - p_m) \quad (6)$$

where φ represents the median, η represents steepness, and p_m (mmHg) and p_M (mmHg) denote minimum and maximum values, respectively. Finally, the time for onset of relaxation is modeled by

$$\beta = \frac{n+m}{n} t_p(H) \quad (7)$$

which is obtained by recognizing that t_p is related to the parameter β in the isovolumic pressure model (3). Initial values for all parameters were obtained from the work by Ottesen and Danielsen (33), in which parameters were based on data from dogs. To obtain human values for the young subject studied in this work, we identified the parameters in Table 1 during our model validation.

Nonlinear Resistances

To our knowledge, previous modeling contributions (see the introduction) assume that, during steady state (i.e., sitting, for $t \leq 60$ s), the small resistances between compartments that represent large conduit vessels are constant. Nevertheless, from the theory of fluid mechanics, it is well known that the resistance depends on the radii of the vessels and that the radii themselves depend on the corresponding transmural pressure.

Our investigation has shown that such dependencies are important to include in regions that represent vessels with large diameters and high blood pressure (i.e., large arteries), whereas they are less important in regions of low blood pressure (i.e., the venous system). Furthermore, these "passive" changes in diameters are also negligible in regions with small vessels (i.e.,

small arteries and arterioles), where autonomic responses are active and dominate the change in vessel diameters. Our previous work (29) did not include nonlinear arterial resistances; therefore, we were not able to obtain a sufficiently wide pulse pressure immediately after postural change from sitting to standing.

Table 1. Steady-state parameters before and after optimization

	Initial	Optimized
<i>Resistance/compliance</i>		
R_{av}	0.030	0.1149
R_{au}	0.072	0.1853
R_{al}	0.087	0.0043
R_{af}	0.183	0.5456
R_{ac}	0.409	0.3177
R_{aup}	1.565	1.8565
R_{alp}	6.522	7.5854
R_{afp}	17.5	17.8953
R_{acp}	6.696	7.0838
R_{mv}	0.007	0.0164
R_v	0.033	0.0368
R_{vu}	0.001	0.000
R_{vi}	0.174	0.1193
R_{vc}	0.957	1.2875
C_a	0.084	0.0732
C_{au}	0.6160	0.7255
C_{al}	0.940	0.9881
C_{af}	0.174	0.2353
C_{ac}	0.159	0.0892
C_v	2.931	2.5181
C_{vu}	15.276	15.4531
C_{vi}	6.038	6.2778
C_{vc}	2.847	2.3007
$fact$	0.1415	0.2079
α	1.4287	2.3220
<i>Heart</i>		
a_v	0.0003	0.0009
b_v	5	4.9122
c_v	6.4	6.9100
d_v	1	0.8310
n_v	2	3.6659
m_v	2.2	1.7369
v_v	9.9	11.0201
θ_v	0.951	0.9213
η_v	17.5	17.6658
φ_v	1	1.1560
$T_{m,v}$	0.186	0.1310
$T_{M,v}$	0.280	0.2305
$P_{m,v}$	0.842	1.1074
$P_{M,v}$	1.158	1.2385
a_a	0.002	0.0002
b_a	5	4.1074
c_a	6.4	6.4325
d_a	1	1.1668
n_a	1.9	1.9501
m_a	2.2	1.9767
v_a	9.9	10.8595
θ_a	6.2778	1.9998
η_a	17.5	16.5386
φ_a	1	2.1152
$T_{m,a}$	0.186	0.2487
$T_{M,a}$	0.280	0.3560
$P_{m,a}$	0.842	1.0065
$P_{M,a}$	0.990	1.2100

Resistances (mmHg·s·cm⁻³) are used in Eq. 1, compliances (cm³/mmHg) in Eq. 2, and heart parameters in Eq. 3. α , Weight for exponent needed to compute mean arterial pressure; see Glossary for other abbreviations.

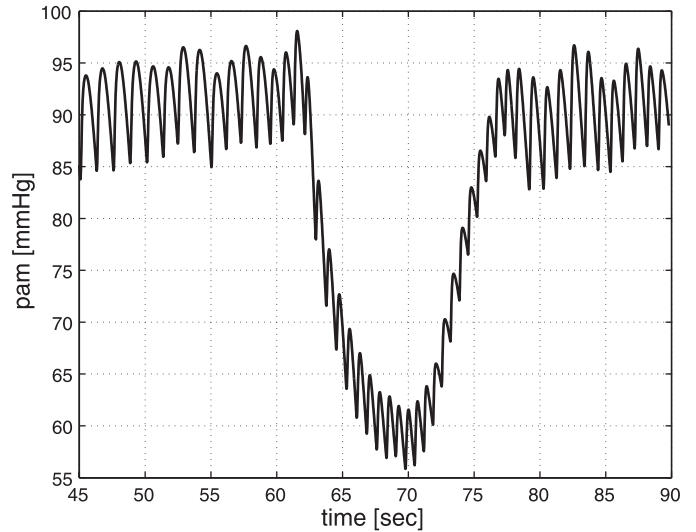


Fig. 2. Mean arterial pressure, $\bar{p}_a(t)$ (p_{am}), for $45 \leq t \leq 90$ s, computed as a continuous function by solving differential Eq. 16. Similar results were obtained for $\bar{p}_{au}(t)$.

To model nonlinearities for these resistances, we base our derivation on Poiseuille's law. For flow in a cylinder with circular cross-sectional area, Poiseuille's law predicts the resistance to flow (14) as

$$R = \frac{8\eta l}{\pi r^4}$$

where R (mmHg·s·cm⁻³) is resistance, r (cm) is radius of the vessel, η (mmHg·s) is viscosity of blood, and l (cm) is length of the cylindrical vessel. If it is assumed that length of the vessel is constant

$$\frac{1}{R} \propto r^4 \propto V^2 \propto p^2 \tag{8}$$

The first relation comes from Poiseuille's law, the second can be obtained by assuming a fixed length l , and the third can be obtained by assuming the validity of the pressure volume relation $V = Cp$. In the compartmental model discussed above each compartment, a number of vessels are lumped together; as a result, we have no specific information about r . The relation in Eq. 8 implies that the resistance is inversely proportional to pressure squared. For real arteries and veins, the resistance will have maximum and minimum values. Hence, we have chosen to model this nonlinear relation using a sigmoidally decreasing function of the form

$$R = (R_M - R_m) \frac{\alpha_2^k}{p^k + \alpha_2^k} + R_m \tag{9}$$

where R_M (mmHg·s·cm⁻³) and R_m (mmHg·s·cm⁻³) are the maximum and minimum values for resistance and p (mmHg) is the blood pressure in the compartment that precedes the resistance. [In our implementation, the actual blood pressure oscillates too much; therefore, for numerical stability, we base the prediction of R on the corresponding mean arterial blood pressure, $\bar{p}(t)$ (mmHg).] As shown in Fig. 2, the mean arterial blood pressure oscillates with the same frequency but with smaller amplitude than p_a ; k represents the steepness of the

sigmoid, and the parameter α_2 is calculated to ensure that R returns to the value of the controlled parameter found during steady state. For $k = 2$, the slope of the sigmoid approximates the relation in Eq. 8. However, the relation in Eq. 8 is valid only for a steady flow. Blood flow in arteries is unsteady, and the flow through a given vessel depends on the state of the vessel. Consequently, as shown in Table 2, we should not expect that $k = 2$.

In our *model 3*, resistances are computed as functions of pressure: $R_{al}(\bar{p}_{au})$, $R_{ac}(\bar{p}_a)$, and $R_{af}(\bar{p}_a)$. The resistance of the aorta (R_{au}) could also be modeled using this method. Initial investigations showed that other mechanisms, e.g., autoregulation or autonomic regulation, may also affect R_{au} . As a consequence, we have used an empirical model to estimate R_{au} (see MODELING AUTONOMIC REGULATION AND CEREBRAL AUTOREGULATION. *Cerebral autoregulation*).

Gravitational effect. Gravitational effects are essential during postural change from sitting to standing. Consider a cylindrical vessel with length Δz (cm) and time-invariant cross-sectional area A (cm²), i.e., $dA/dt = 0$. Assume that there is no velocity across the vessel and that the blood pressure is only a function position along the vessel. Hence, $dv/dr = 0$, where v (cm/s) and r (cm) denote the velocity and radii, respectively, and the volumetric flow rate becomes $q = Av$ (cm³/s). Finally, assume that the drag force due to viscous shear is proportional to q . Thus the drag force per cross-sectional area unit is proportional to q ; i.e., the drag force can be written as $-RAq$, where R (mmHg·s·cm⁻³) may be interpreted as the resistance. In steady state, the resistance R is given by Poiseuille's law (23)

$$R = \frac{8\pi\eta\Delta z}{A^2}$$

To derive the mathematical model, we proceed by balancing inertial forces with the drag force, the pressure force, and the gravitational force. The inertial force is given by

$$M \frac{dv}{dt} = \rho A \Delta z \frac{d}{dt} \left(\frac{q}{A} \right) = \rho \Delta z \frac{dq}{dt}$$

where $\rho = 1.055$ (g/cm³) is the density of the fluid and M (g) is the mass of the fluid contained in a piece of the vessel with length Δz (cm) and cross-sectional area A (cm²; Fig. 3). Thus Newton's second law, which describes balancing of forces, gives

$$\rho \Delta z \frac{dq}{dt} = (p_{in} - p_{out})A + Mg \cos(\psi) - RAq$$

where $g = 981$ (cm/s²) is the gravitational acceleration. From this, it follows that

$$L \frac{dq}{dt} = p_{in} - p_{out} + \rho g \Delta h - RAq \quad (10)$$

where $L = \rho \Delta z / A$ (1/s²) is the inertance and $\Delta h = \Delta z \cos(\psi) = h_{in} - h_{out}$ (cm) is the vertical difference of the vessel inlet (at h_{in} where p_{in} and p_{out} represent pressure at the inlet and outlet, respectively). During steady state, Eq. 10 reduces to

Table 2. *Optimized parameters*

	Initial	Optimized
p_a	92.8	
p_{au}	90.0	
τ_{cv}	10.00	18.57
τ_{ca}	10.00	13.67
τ_R	5.0	23.03
τ_s	5.0	0.076
h_H	50.0	46.73
h_k	3.0	3.92
δ	0.4	1.26
k (R_{ai})	5.0	1.48
R_M (R_{ai})	$4 \times R_{al}^{ss}$	1.69
R_m (R_{ai})	$R_{ai}^{ss}/4$	1.1×10^{-3}
k (R_{ac})	5.0	8.79
R_M (R_{ac})	$4 \times R_{ac}^{ss}$	2.49
R_m (R_{ac})	$R_{ac}^{ss}/4$	1.3×10^{-2}
k (R_{af})	5.0	3.83
R_M (R_{af})	$4 \times R_{af}^{ss}$	0.15
R_m (R_{af})	$R_{af}^{ss}/4$	2.9×10^{-5}
k (R_{aup})	5.0	5.74
R_M (R_{aup})	$4 \times R_{aup}^{ss}$	14.58
R_m (R_{aup})	$R_{aup}^{ss}/4$	0.13
k (R_{aip})	5.0	10.57
R_M (R_{aip})	$4 \times R_{aip}^{ss}$	145.19
R_m (R_{aip})	$R_{aip}^{ss}/4$	0.41
k (R_{afp})	2.0	3.69
R_M (R_{afp})	$4 \times R_{afp}^{ss}$	64.81
R_m (R_{afp})	$R_{afp}^{ss}/4$	0.16
k (c_v)	2.0	4.62
R_M (c_v)	$4 \times c_{vtr}^{ss}$	17.27
R_m (c_v)	$c_{vtr}^{ss}/4$	1.04
k (c_a)	2.0	4.58
R_M (c_a)	$4 \times c_{vtr}^{ss}$	11.99
R_m (c_a)	$c_{vtr}^{ss}/4$	0.94
k (C_a)	2.0	0.38
C_M (C_a)	$4 \times C_a^{ss}$	4.3×10^{-2}
C_m (C_a)	$C_a^{ss}/4$	4.8×10^{-4}
k (C_{au})	2.0	17.22
C_M (C_{au})	$4 \times C_{au}^{ss}$	1.01
C_m (C_{au})	$C_{au}^{ss}/4$	0.42
k (C_{ai})	2.0	13.90
C_M (C_{ai})	$4 \times C_{al}^{ss}$	15.25
C_m (C_{ai})	$C_{al}^{ss}/4$	0.82
k (C_{ac})	2.0	4.05
C_M (C_{ac})	$4 \times C_{ac}^{ss}$	0.23
C_m (C_{ac})	$C_{ac}^{ss}/4$	7.0×10^{-2}
k (C_{af})	2.0	81.34
C_M (C_{af})	$4 \times C_{af}^{ss}$	0.46
C_m (C_{af})	$C_{af}^{ss}/4$	1.7×10^{-2}
k (C_v)	3.0	0.47
C_M (C_v)	$5 \times C_v^{ss}$	15.32
C_m (C_v)	C_v^{ss}	0.52
k (C_{vu})	3.0	12.90
C_M (C_{vu})	$5 \times C_{vu}^{ss}$	55.86
C_m (C_{vu})	$C_{vu}^{ss}/5$	1.93
k (C_{vi})	3.0	47.93
C_M (C_{vi})	$5 \times C_{vl}^{ss}$	277.94
C_m (C_{vi})	$C_{vl}^{ss}/5$	0.17
k (C_{cv})	3.0	15.71
C_M (C_{cv})	$5 \times C_{vc}^{ss}$	13.89
C_m (C_{cv})	$C_{vc}^{ss}/5$	0.19

Constants \bar{p}_a and \bar{p}_{au} denote pressure set points used in control equations. Time constants (τ_i) denote time delay involved with controlled variables. Parameters for gravity denote maximum height needed to obtain observed pressure drop, and a small delay (δ) from which the subjects stands up. Optimized values for resistances and capacitors include k_i , which represent the steepness of the sigmoid, and a maximum (R_M or C_M) and a minimum (R_m or C_m) value. Optimized values for R_{au} and R_{ac} are shown in Figs. 4 and 5. Steady state; see *Glossary* for other abbreviations.

$$q = \frac{(p_{in} + \rho gh_{in}) - (p_{out} + \rho gh_{out})}{R} \quad (11)$$

When modeling postural change from sitting to standing, we substitute Eq. 11 for Kirchhoff's current law. In the limit $g \rightarrow 0$, Eq. 11 approaches the normal form of Kirchhoff's current law given in Eq. 1. In the case of energy conservation ($R \rightarrow 0$), Bernoulli's law for steady flow is recovered; as a result, $p_{in} + \rho gh_{in} = p_{out} + \rho gh_{out}$. Thus Kirchhoff's current law is still valid if we interpret p as the hydrostatic pressure $p + \rho gh$.

To capture the transition from sitting to standing, h is defined for the lower body compartments as the exponentially increasing function

$$h(t) = \frac{h_M}{1 + e^{-k(t - T_{up} - \delta)}} \quad (12)$$

where T_{up} (s) is the time at which the subject stands up, h_M (cm) is the maximum height needed for the mean arterial blood pressure in the finger to drop as indicated by the data, and δ (s) is the latency for the transition to standing. In our experiments, the subjects sit with their legs elevated and the hand, where the pressure is measured, held by a sling at the level of the heart. Therefore, compartments that represent the heart and the finger are not affected by gravity. Compartments that represent the brain and the upper body are exposed to constant hydrostatic conditions, which are neglected in the current formulation. However, compartments that represent the legs are affected by gravity. Consequently, equations for the flows q_{al} and q_{vl} will be modified as described in Eq. 11

$$q_{al} = \frac{p_{au} - (p_{al} + \rho gh)}{R_{al}}$$

$$q_{vl} = \frac{(p_{vl} + \rho gh) - p_{vu}}{R_{vl}}$$

In the first of these equations, $h_{in} = 0$ and $h_{out} = h$, where h is computed using Eq. 12. In the second of these equations, $h_{in} = h$ and $h_{out} = 0$.

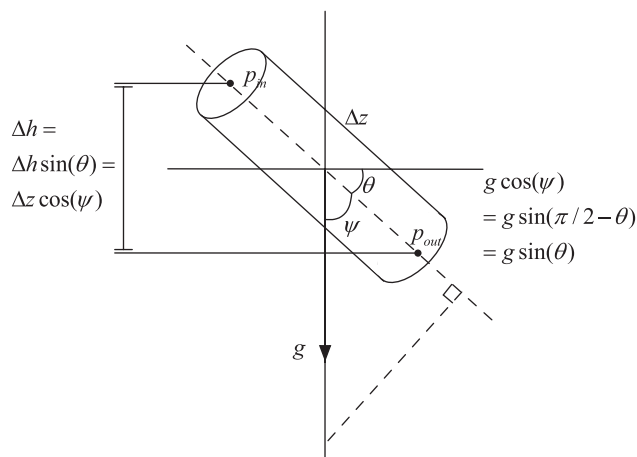


Fig. 3. Vessel segment with cross-sectional area A (cm²) and length Δz (cm). At one end, pressure is p_{in} (mmHg); at the other end, pressure is p_{out} (mmHg). Vessel is at an angle θ with respect to gravity g (g/cm²) and at an angle ψ with respect to the horizontal axis. Difference in vertical latitude is $\Delta h = \Delta z \cos(\psi)$ (cm).

MODELING AUTONOMIC REGULATION AND CEREBRAL AUTOREGULATION

Two main control mechanisms play a role: autonomic regulation and cerebral autoregulation. Autonomic regulation is mediated via the autonomic nervous system and causes changes of resistances in the vascular bed, compliance, heart rate, and cardiac contractility. Autoregulation is a local control that maintains cerebral perfusion, despite changes in systemic pressure. Autoregulation is mediated via changes in myogenic tone, metabolic demands, and CO₂ concentration.

Autonomic regulation. Autonomic regulation is modeled as a pressure regulation where heart rate (H, beats/s), cardiac contractility (c_a and c_v , mmHg/cm³), peripheral systemic resistance (R_{aup} and R_{alp} , mmHg·s·cm⁻³), and systemic compliance (C_a , C_{au} , C_{al} , C_{ac} , C_{af} , C_v , C_{vu} , C_{vl} , and C_{vc} , cm³/mmHg) are functions of mean arterial blood pressure (\bar{p}_a , mmHg).

The change in the controlled parameters is modeled using a first-order differential equation with a set-point function dependent on \bar{p}_a

$$\frac{dx(t)}{dt} = \frac{-x(t) + x_{ctr}(\bar{p}_a)}{\tau} \quad (13)$$

This simple model is able to predict the observed dynamics. The parameter $x(t)$ is controlled, $x_{ctr}(\bar{p}_a)$ is the set-point function, and τ (s) is a time constant that characterizes the time required for the controlled variable to obtain its full effect. Different values of τ were used for control of cardiac contractility, compliance, and resistance (Table 2). As described earlier, autonomic regulation yields increases in peripheral vascular resistance, heart rate, and cardiac contractility. Heart rate is directly obtained from data. Hence, it is not modeled using the set-point function (13). To obtain increases in peripheral resistances (R_{aup} , R_{alp} , and R_{afp}) and cardiac contractility (c_{la} and c_{lv}) in response to the decrease in arterial blood pressure, the following set-point function has been used

$$x_{ctr}(\bar{p}_a) = (x_M - x_m) \frac{\alpha_2^k}{\bar{p}_a^k + \alpha_2^k} + x_m \quad (14)$$

A sigmoidal function was used, because it displays saturation; i.e., the function has a maximum and a minimum value corresponding to maximum dilation and maximum constriction of the vessels. In addition, vascular tone is increased, leading to a decrease in compliance in response to a decrease in arterial blood pressure. Hence, for compliance, the set-point function has the form

$$x_{ctr}(\bar{p}_a) = (x_M - x_m) \frac{\bar{p}_a^k}{\bar{p}_a^k + \alpha_2^k} + x_m \quad (15)$$

Equation 14 gives rise to a decreasing sigmoidal curve (i.e., for a decreasing pressure, the value of x_{ctr} will increase), whereas Eq. 15 gives rise to an increasing sigmoidal curve (i.e., for a decreasing pressure, the value of x_{ctr} will decrease). The parameters x_m and x_M are minimum and maximum values for the controlled parameter $x(t)$. The parameter α_2 is calculated to ensure that $x(t)$ returns the value of the controlled parameters found during steady state. Initial values of parameters for k , x_m , and x_M are from Danielsen (5) (Table 2).

These control equations (Eqs. 13–15) are formulated as functions of mean arterial blood pressure. However, our model describes the instantaneous (pulsatile) pressure. Mean values are computed as weighted averages, where the present is weighted higher than the past

$$\bar{p}_a = \frac{1}{N} \int_0^t p_a(s) e^{-\psi(t-s)} ds \tag{16}$$

The normalization factor N is introduced to ensure that the correct mean arterial blood pressure is obtained for $p_a = 1$, i.e.,

$$N = \int_0^t e^{-\psi(t-s)} ds = \frac{1 - e^{-\psi t}}{\psi} \tag{17}$$

Because our mathematical model is described by differential equations, it is more efficient to implement a differential equation to compute the mean arterial blood pressure. Hence, we differentiate Eq. 16 to obtain

$$\frac{d\bar{p}_a}{dt} = \frac{-\bar{p}_a + p_a(t)}{\tau} \tag{18}$$

A similar equation is used to calculate p_{au} .

Cerebral autoregulation. On the transition to standing, cerebral autoregulation mediates a decline in cerebrovascular resistance (R_{acp}) in response to the decrease in arterial blood pressure. In addition, the autonomic system may also play a role, by decreasing the cerebrovascular resistance due to cholinergic vasodilation or by increasing the resistance due to release of norepinephrine (7). Consequently, it is not trivial to develop an accurate physiological model that describes cerebral autoregulation. Our strategy in this work has been to use a piecewise linear function with unknown coefficients to obtain a representative function that describes the time-varying response of the cerebrovascular resistance. Once such a function is obtained, we can interpret the result in terms of the underlying physiology. To obtain such a function, we have parameterized the cerebrovascular resistance using piecewise linear functions of the form

$$R_{acp}(t) = \sum_{i=1}^n \gamma_i H_i(t) \tag{19}$$

where H_i represents the standard “hat” functions given by

$$H_i(t) = \begin{cases} \frac{t - t_{i-1}}{t_i - t_{i-1}}, & t_{i-1} \leq t \leq t_i \\ \frac{t_{i+1} - t}{t_{i+1} - t_i}, & t_i \leq t \leq t_{i+1} \\ 0, & \text{otherwise} \end{cases} \tag{20}$$

The unknown coefficients γ_i will be estimated together with the other control parameters in Table 2. As described above, we have used a similar method to estimate the resistance R_{au} , which may be affected by passive nonlinear resistances and autonomic regulation.

PARAMETER ESTIMATION

Estimation of model parameters has been done in a number of steps. First, we used physiological properties of the system

to determine initial values for all parameters and variables (Table 1). Then we solved the steady-state problem (without including effects of gravity and regulation); i.e., we solved 11 equations of the form of Eq. 2, one for each compartment. During steady state, all resistances and capacitors were kept constant; hence, terms that involve $p(dC)/dt = 0$. These equations are combined with Eqs. 3–7, which determine pressures in the left atrium and ventricle, and Eq. 18, which determines the mean arterial pressures \bar{p}_a and \bar{p}_{au} . Finally, we estimated a constant factor used to calculate cerebral blood flow velocity $v_{acp} = q_{acp}/\text{fact}$ (cm/s). We have used a constant factor (fact), because we assume that the cross-sectional area of the middle cerebral artery does not change significantly (36). These equations involve a total of 53 parameters that were estimated using a nonlinear optimization method, the Nelder-Mead algorithm, which is based on function information computed on sequences of simplexes (13). Estimated parameter values are shown together with initial values in Table 1. To obtain the best possible parameter values, we used the following cost function to minimize the difference between measured and computed values of cerebral blood flow velocity and finger pressure

$$J = \frac{1}{N\bar{v}^d} \sum_{i=1}^N (v_i^d - v_i^c)^2 + \frac{1}{N\bar{p}^d} \sum_{i=1}^N (p_i^d - p_i^c)^2 + \frac{1}{M\bar{v}^{d,dia}} \sum_{i=1}^M (v_i^{d,dia} - v_i^{c,dia})^2 + \frac{1}{M\bar{v}^{d,sys}} \sum_{i=1}^M (v_i^{d,sys} - v_i^{c,sys})^2 + \frac{1}{M\bar{p}^{d,dia}} \sum_{i=1}^M (p_i^{d,dia} - p_i^{c,dia})^2 + \frac{1}{M\bar{p}^{d,sys}} \sum_{i=1}^M (p_i^{d,sys} - p_i^{c,sys})^2$$

where $v = v_{acp}$ and $p = p_{af}$. The superscripts d and c refer to data and corresponding computed values, respectively. In the first two sums, $i = [1:N]$, where N is the number of data points. To compare the computed values x_c and the measured data values x_d ($x = v, p$), interpolation is used to evaluate the computed value at the same points in time where the data are obtained. Each term is divided by the number of points and the mean value of the measured data. Our model is not able to predict second-order oscillations (see Fig. 7B). The error due to poor resolution of second-order oscillations is of the same order of magnitude as the error due to poor resolution of the maximum and minimum values. However, for our modeling purpose, it is important to resolve the maximum and minimum values, but it is not important to resolve second-order oscillations. To reward good resolution of the maximum and minimum values, we have added four additional sums predicting the error between systolic and diastolic (sys and dia , respectively) computed and measured values of v_{acp} and p_{af} . Because of the nature of the pulse wave, only one minimum and maximum value is obtained per period; hence, $i = [1:M]$, where M is the number of periods for $45 \leq t \leq 90$ s.

After the steady-state parameters (constant values of all resistances and compliances) were obtained, we included all equations that describe the control and ran another optimization to fit parameters that describe the control functions. This second optimization included 27 ordinary differential equa-

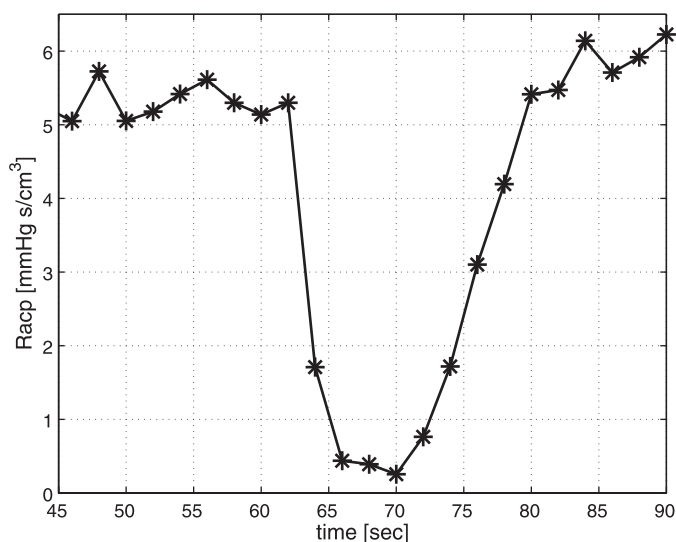


Fig. 4. Cerebral vascular resistance [$R_{acp}(t)$] for $45 \leq t \leq 90$ s, computed using piecewise linear Eq. 19. *, 26 values used to estimate cerebrovascular resistance. Shortly after transition to standing (at $t = 60$ s), cerebral autoregulation leads to a decrease in cerebrovascular resistance followed by an increase to a new steady-state value slightly higher than the steady-state value during sitting (for $t \leq 60$ s).

tions: 11 of the form of Eq. 2, 2 of the form of Eq. 18, and 14 of the form of Eq. 13. These equations are solved together with the heart model described in Eqs. 3–7, equations for passive nonlinear resistances (Eq. 9), Eq. 12, which determines the height used to calculate gravitational pooling in the veins, and the piecewise linear functions used to parameterize R_{acp} and R_{au} . This second optimization gave rise to a total of 111 parameters that were optimized: 59 parameters are shown in Table 2, and 52 parameters used to parameterize R_{acp} and R_{au} are shown in Figs. 4 and 5. During this second optimization, all parameters found during steady-state (i.e., during sitting, for $t < 60$ s) optimization remained constant (at the optimized values). In general, the inverse problem for parameter estimation does not provide a unique solution. In addition, the optimized parameters depend on the initial guesses and on the optimization algorithm.

The differential equations from our mathematical model, Eqs. 2, 13, and 18, are solved using MATLAB's (MathWorks, Natick, MA) differential equations solver "ode15s." Initial values for the resistance and compliance parameters were found from the distribution of the total blood volume between compartments and steady-state estimates for the pressure values in the various compartments. The blood volume distribution is obtained using the quantities suggested by Beneken and DeWit (3). Initial values for the resistances and compliances were based on previously reported values for blood volumes and flow rates (3), whereas blood pressure values were obtained from standard physiology literature (4). Volumes for each compartment are given by

$$V = Cp + V_{unstr}$$

where V_{unstr} is the unstressed volume, i.e., the part of the volume that is not pumped out during the cardiac cycle. Therefore, initial values for compliance and resistance are calculated by

$$C = \frac{V - V_{unstr}}{p}$$

$$R = \frac{P_{in} - P_{out}}{R}$$

These initial values are given in Table 1. Initial values for pressures and unstressed volumes are given in Table 3.

EXPERIMENTAL DATA

Our model was validated against continuous physiological data from a young subject during the transition from sitting to standing. In particular, we used arterial blood pressure mea-

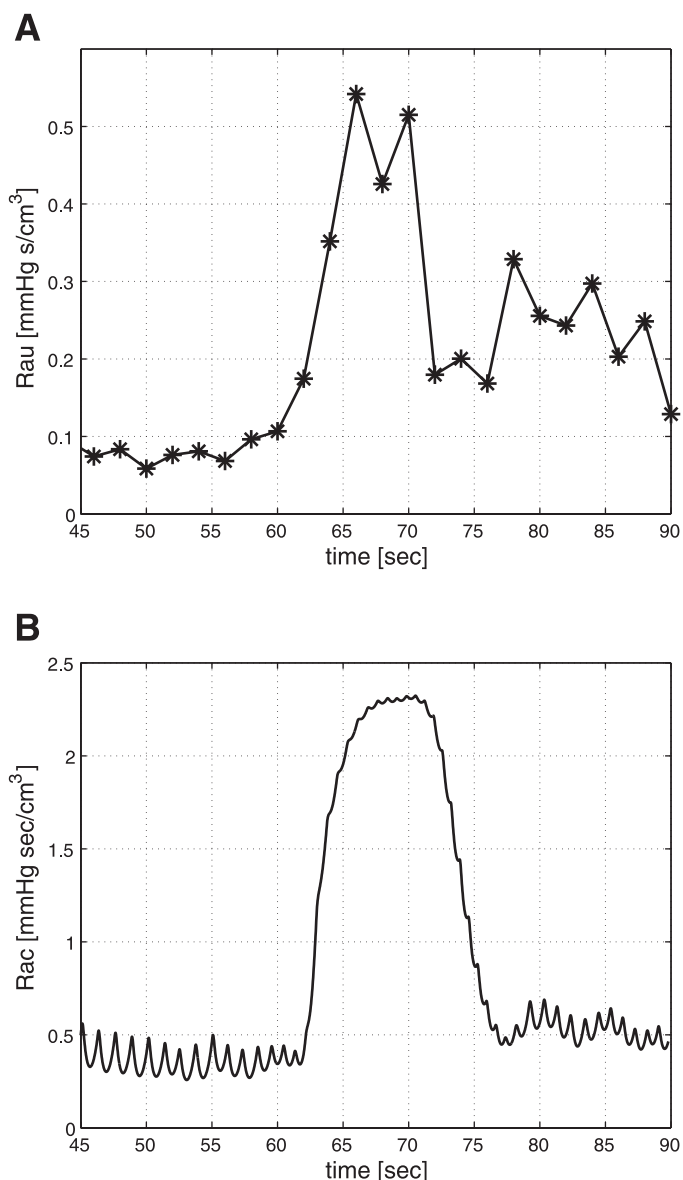


Fig. 5. "Passive" resistances between compartments that represent large arteries. A: $R_{au}(t)$ fitted, using Eq. 19, with 26 values (*). B: $R_{ac}(t)$ computed using Eq. 9. R_{au} and R_{ac} are depicted for $45 \leq t \leq 90$ s. R_{au} and R_{ac} increase in response to decreasing pressure and then decrease to a new steady-state value. Models for $R_{ai}(t)$ and $R_{aj}(t)$ are similar to that for $R_{ac}(t)$ and show similar trends.

Table 3. Initial values for pressures and total and unstressed volumes

Parameter	Value
<i>Pressure, mmHg</i>	
p_a	70.0
p_{au}	72.0
p_{al}	73.0
p_{af}	70.0
p_{ac}	70.0
p_v	2.0
p_{vu}	2.1
p_{vl}	2.2
p_{vc}	43.0
<i>Total volume, cm³</i>	
V_{lv}	68.0
V_{la}	172.0
V_a	40.0
V_{au}	300.0
V_{al}	233.7
V_{af}	80.0
V_{ac}	70.0
V_v	183.2
V_{vu}	1909.5
V_{vl}	724.6
V_{vc}	391.4
<i>Unstressed volume, cm³</i>	
V_{a}^{unstr}	32.0
V_{au}^{unstr}	240.0
V_{al}^{unstr}	151.9
V_{af}^{unstr}	64.0
V_{ac}^{unstr}	56.0
V_v^{unstr}	168.5
V_{vu}^{unstr}	1756.7
V_{vl}^{unstr}	652.1
V_{vc}^{unstr}	360.1

Estimates of initial pressures are based on standard physiology literature texts (4, 7), Estimates of initial volumes are based on the work of Beneken and Dewit (3). unstr, Unstressed; see Glossary for other abbreviations.

measurements from the finger and arterial blood flow velocity measurements from the middle cerebral artery (15). Each subject was instrumented with a three-lead ECG (Collins) to obtain heart rate and a photoplethysmographic cuff on the middle finger of the right hand supported at the level of the right atrium to obtain noninvasive beat-by-beat blood pressure (Finapres, Ohmeda). The middle cerebral artery was insonated by placement of a 2-MHz Doppler probe (Nicolet Companion) over the temporal window to obtain continuous measurements of blood flow velocity. The envelope of the velocity waveform was derived from the fast Fourier transform of the Doppler signal, as described by Aaslid et al. (1). All physiological signals were digitized at 500 Hz (Windaq, Dataq Instruments) and stored for offline analysis. Blood pressure reduction of ~ 30 mmHg on the transition to standing was used as a challenge for cerebral autoregulation. Subjects sat in a straight-backed chair with their legs elevated at 90° in front of them. They were then asked to stand. Standing was defined as the moment both feet touched the floor. Subjects performed two 5-min trials in the sitting position followed by standing for 1 min and one 5-min trial in the sitting position followed by 6 min of standing.

RESULTS

We were able to obtain excellent agreement between simulations and measured data. Figure 6 shows the characteristic features of the measured data. After the transition to standing at $t = 60$ s, blood pressure (systolic, diastolic, and mean values) dropped significantly. At the same time, mean blood flow velocity decreased during the transition from sitting to standing (dark line through pulsatile velocity data). However, although systolic and diastolic values of pressure decreased, only the diastolic value of the blood flow velocity was diminished. The systolic values remained at baseline or were even slightly increased. This yields a significant widening of the pulsatile flow, a feature typical for young people with normal regulatory responses (15).

First, we evaluated our model's ability to reproduce the dynamics during steady state (i.e., during sitting, for $t \leq 60$ s). We applied initial parameter values from physiological considerations (see above). Then we fitted our model [without including equations that describe resistances of large arteries as nonlinear functions of pressure (Eq. 9) and those that describe active control (Eqs. 13 and 19)] to the data set. The duration of the cardiac cycles was obtained from the ECG (Fig. 6). Simulation results in Fig. 7 show that we obtained an excellent agreement between our model and the data during steady state. However, our model is not able to resolve details of the secondary oscillations observed within each cardiac cycle (Fig. 7B), a feature that is not included in our heart model.

The second step in validating our model is to illustrate that we can model effects of venous pooling after the transition to standing. Venous pooling results in dramatic reductions of cerebral blood flow velocity and arterial pressure (Fig. 8): with the parameters listed in Tables 1 and 2, it is possible to decrease blood flow velocity and pressure. Two observations

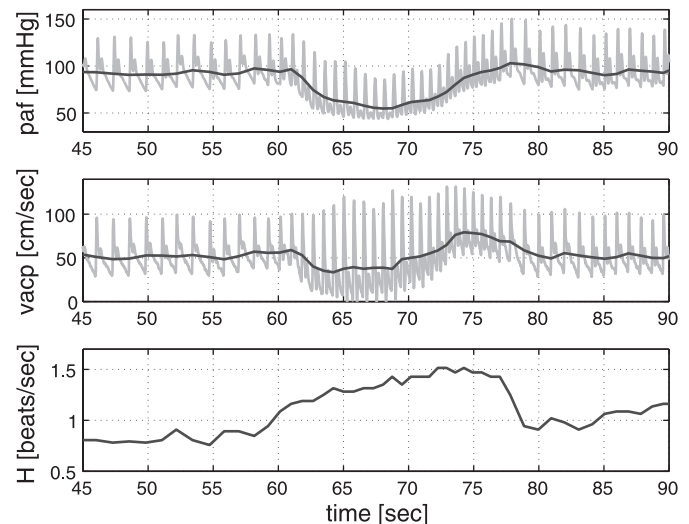


Fig. 6. Measured arterial blood pressure in the middle finger [$p_{af}(t)$], cerebral blood flow velocity [$v_{acp}(t)$], and heart rate [$H(t)$] for a young subject for $45 \leq t \leq 90$ s. Gray traces, time-varying values; dark traces, corresponding beat-to-beat mean values. Heart rate is obtained as follows: $H = 1/T$, where T (s) is cardiac cycle duration. Immediately after transition to standing (at $t = 60$ s), pulsatile and mean blood pressure dropped significantly, mean blood flow velocity dropped, and pulsatile blood flow velocity widened (i.e., systolic value increased, and diastolic value decreased). Initially, heart rate increased and then reached a new steady state at a higher level than during sitting.

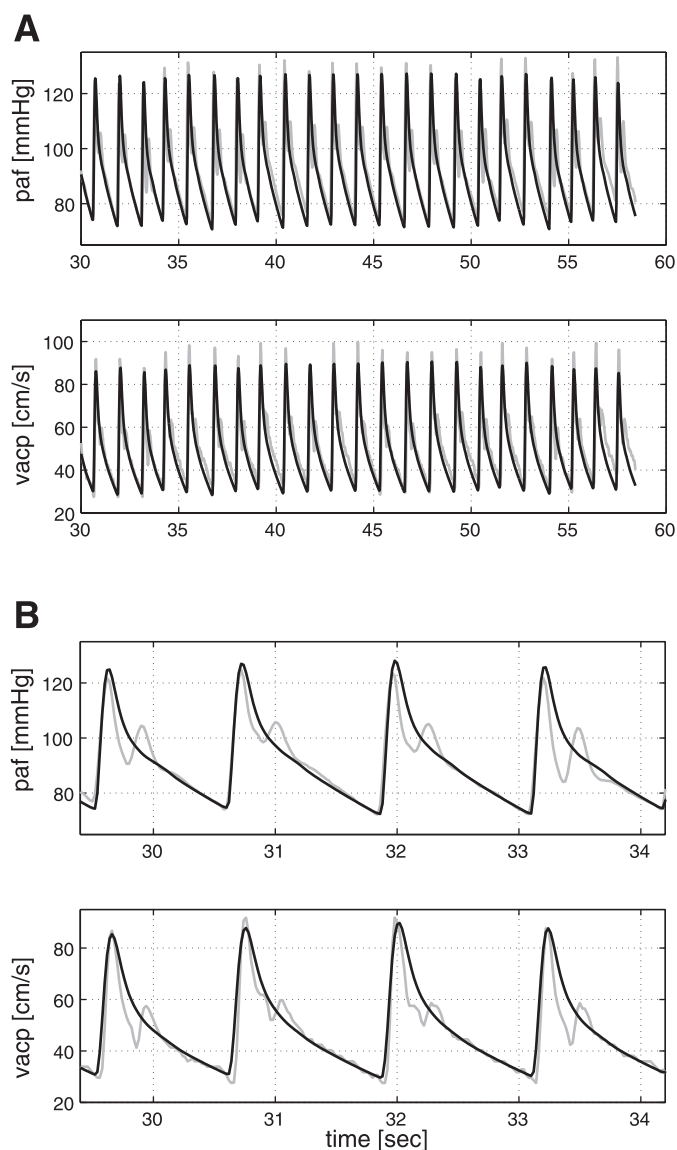


Fig. 7. *A*: middle cerebral blood flow velocity and arterial finger blood pressure during sitting, i.e., for $0 \leq t \leq 60$ s. *B*: magnification of $29.4 \leq t \leq 34.2$ s in *A*. During steady state, $v_{acp}(t)$ and $p_{af}(t)$ were obtained by solving differential equations of the form of Eq. 2 (see APPENDIX for all equations). Dark traces, result of our computations; gray traces, corresponding data. Our model can accurately predict blood flow velocity and blood pressure profiles while the subject is sitting. As shown in *B*, our model is not able to capture secondary oscillations observed in the data.

should be noted: 1) although we did not include effects of the control, we still see an increase in heart rate, because heart rate information is obtained from the data (Fig. 6), and 2) although blood flow velocity and pressure drop immediately after standing (at 60 s), the pulse amplitude for blood flow velocity and pressure remains very narrow.

Next, we demonstrated the impact of the nonlinear relation between pressure and the vascular resistance of the large arteries (see MODELING BLOOD PRESSURE AND BLOOD FLOW VELOCITY. *Nonlinear resistance*); i.e., we let $R_{al}(p_{au})$, $R_{au}(p_a)$, $R_{ac}(p_a)$, and $R_{af}(p_a)$ be functions of pressure. We used the same values for all remaining parameters, and the result of this simulation is shown in Fig. 8*B*. The pulse pressure amplitude

is higher immediately after the transition to standing (from $60 \leq t \leq 65$ s); thus the model better represents measured values (cf. dark lines in Fig. 8, *A* and *B*, in the transition region, for $60 \leq t \leq 65$ s).

The third step involved incorporation of all active control mechanisms. Results that include effects of autonomic regulation and autoregulation are shown in Fig. 9. Our model is able to predict the change in the overall profile during the transition from sitting to standing. The only minor difference is that the data include a slight overshoot in pressure in the transition to standing.

Autonomic regulation was included using a model that predicts parameters as a function of pressure. Although this

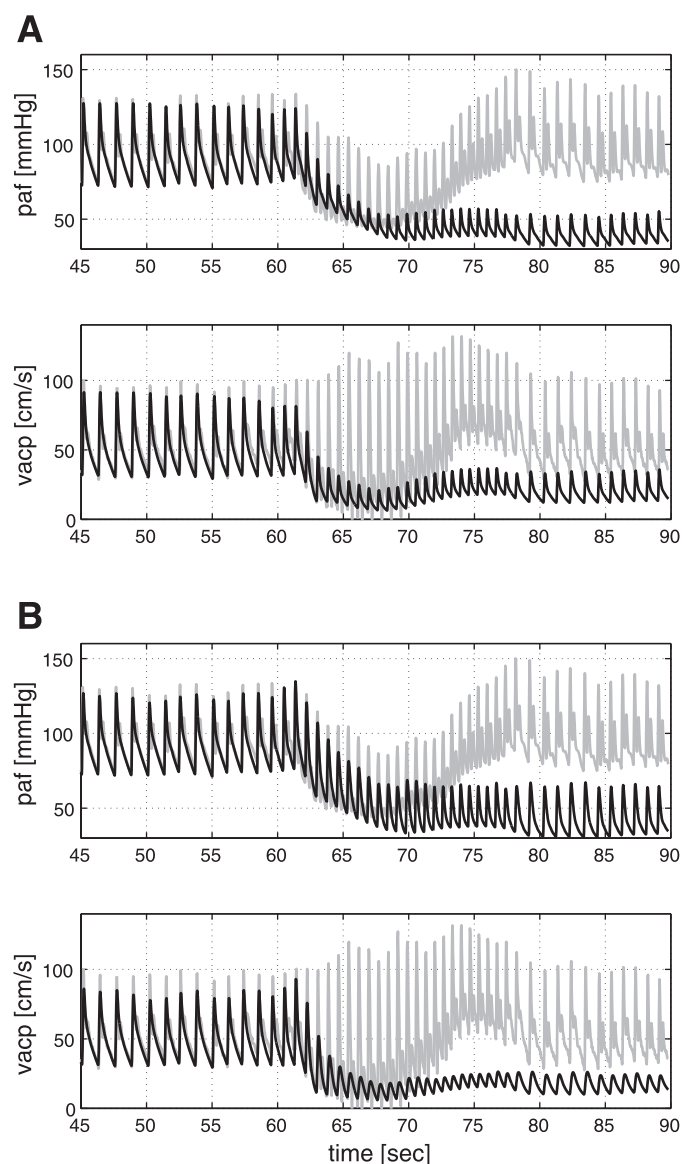


Fig. 8. Cerebral blood flow velocity and arterial finger blood pressure for $45 \leq t \leq 90$ s. Effect of standing is shown without active control mechanisms. *A*: blood flow velocity and blood pressure (dark traces) decrease as a result of redistribution of volumes from changes in hydrostatic pressure. Results were obtained by solving equations of the form of Eq. 2, where gravity is included, as shown in Eq. 11. *B*: effect of including nonlinear functions of pressure for large arterial resistances as described in Eq. 9. Immediately after standing (from $60 \leq t \leq 65$ s), pulse pressure is much wider. Dark traces, simulated model results; gray traces, data.

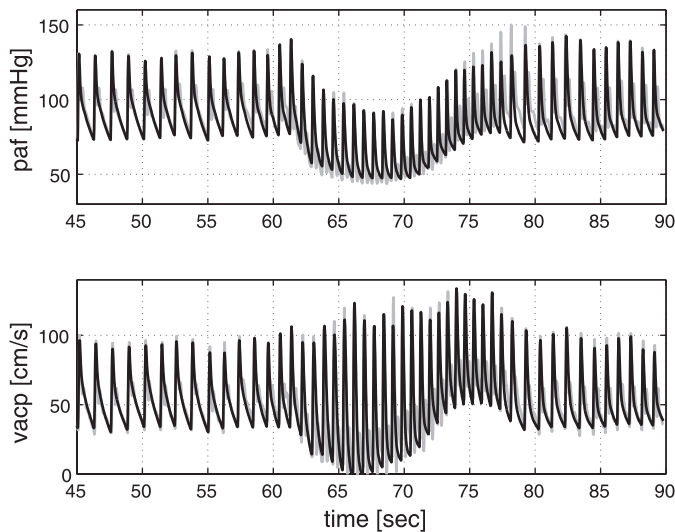


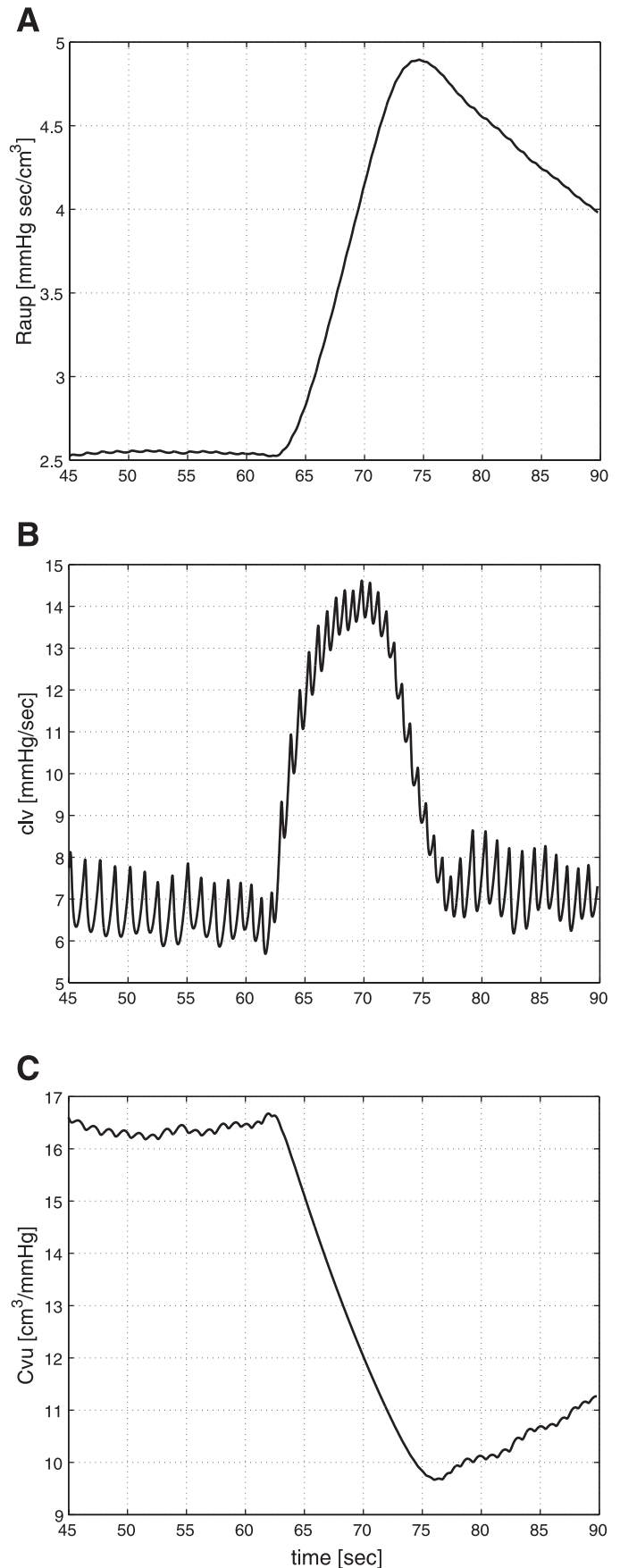
Fig. 9. Autonomic regulation and cerebral autoregulation of arterial finger blood pressure and cerebral blood flow velocity for $45 \leq t \leq 60$ s. Model is able to reproduce data well. Dark traces, model simulations; gray traces, data. Results were obtained by solving cardiovascular equations of the form of Eq. 2, including gravity, as described in Eq. 11, passive resistances (Eq. 9), and autonomic regulation and cerebral autoregulation (Eqs. 13 and 19). The main region, where the model does not capture the dynamics of the data, is just before return to steady state during standing, i.e., for $t \sim 60$ s.

method does not incorporate effects of sympathetic vs. parasympathetic activation, it does include net effects of neurogenic regulation. Effects of cerebral autoregulation were modeled using the empirical model described in Eq. 19. We chose to include 26 points to represent the dynamics of cerebral vascular resistance, R_{acp} (Fig. 4). Figure 4 shows that R_{acp} decreases because of autoregulation in response to the decrease in pressure. From earlier work (27), we expected an initial increase before the decrease; however, the model used in our previous work was much simpler than the model used in the present work. In particular, the parameter that represents peripheral resistance (R_p) in our earlier work lumps the peripheral resistance from the entire body, i.e., it combines R_{acp} , R_{aup} , R_{afp} , and R_{alp} . Consequently, it can be difficult to use R_p to describe the dynamics of the cerebrovascular resistance R_{acp} , as we attempted to do in our earlier work.

The resistance of the upper body (R_{au}) was also modeled using a piecewise linear model with unknown parameters, as described elsewhere (19). We expected that R_{au} may depend on autonomic regulation and may be a nonlinear passive function of pressure. This resistance follows trends predicted by remaining resistances that represent the large arteries (Fig. 5).

Finally, Fig. 10 depicts the dynamics of some of the controlled variables, e.g., arterial resistance (R_{aup}), cardiac con-

Fig. 10. Dynamics of controlled variables for $45 \leq t \leq 90$ s. A: peripheral resistance in the upper body [$R_{aup}(t)$]. B: cardiac contractility of the left ventricle [$c_{lv}(t)$]. C: compliance of veins in the upper body [$c_{vu}(t)$]. Results were obtained by solving Eq. 13 together with equations for the cardiovascular system (Eq. 2). Autonomic regulation yields increase in peripheral resistance, cardiac contractility, and vascular tone. The latter yields a decrease in compliance as shown. Timing of the different controls varies; especially, note that cardiac contractility changes faster than resistances and capacitances. Regulation of the remaining resistances, contractility, and compliances showed similar responses.



tractility of the left ventricle (c_{lv}), and venous compliance in the upper body (C_{vu}). These results display quite different dynamics of the three types of variables. In particular, the compliance and peripheral resistance do not reach a steady state during the 10 s after the transition from sitting to standing (from $80 \leq t \leq 90$ s), perhaps because the dynamics that change the ventricular contractility occur over a much faster time scale than those that affect resistances and compliances. Finally, the dynamics of other resistances, capacitors, and atrial contractility are similar to the parameters shown in Fig. 10.

CONCLUSION

In summary, we have developed an 11-compartment model that can predict cerebral blood flow velocity and finger blood pressure. This model includes a physiological description of dynamics as a response to hydrostatic pressure changes during postural change from sitting to standing. Furthermore, our model includes nonlinear functions describing resistances of the large systemic arteries as functions of pressure. To regulate blood pressure and cerebral blood flow velocity after postural change from sitting to standing, our model includes autonomic regulation using first-order differential equations regulating cardiac contractility, peripheral resistance, and vascular tone (compliance). Furthermore, we have included an empirical model describing the dynamics of cerebral vascular resistance. Validation of our model against one data set showed that, by including the mechanisms described above, our model is able to reproduce the dynamics of blood flow velocity and blood pressure needed to compensate for hypotension observed during postural change from sitting to standing.

Modeling of physiological responses to standing enables a better understanding of physiological mechanisms underlying disorders related to orthostatic tolerance, e.g., orthostatic hypotension and syncope. Our model predicts that, in the absence of regulatory mechanisms (Fig. 8), blood pressure and blood flow velocity declined on the transition to standing and did not recover to baseline in the upright position. This modeling result has not been validated against data. However, similar responses have been observed clinically. For example, sustained blood pressure reduction in the upright position is seen in clinical syndromes with orthostatic hypotension associated with autonomic failure (16, 17). Different etiologies and severity of autonomic failure may lead to differences in pathophysiological responses during the transition to standing. For example, severe peripheral autonomic failure, such as pure autonomic failure or diabetic neuropathy, may be associated with orthostatic hypotension with no heart rate increment. Cerebral autoregulation, which maintains cerebral perfusion over a wide range of pressure (25), may be preserved, expanded, or reduced in orthostatic hypotension. However, cerebral blood flow would decline with impairment of autoregulation and/or when blood pressure is diminished below the autoregulated range. A transient impairment of autonomic and cerebral blood flow control is common in young people with vasodepressor syncope. This is associated with a withdrawal of sympathetic tone followed by a decline of blood pressure and cerebral perfusion (12, 22, 24).

Furthermore, our results show that, by including passive nonlinear responses of resistances in the large arteries, we can obtain sufficient widening of the pulse pressure amplitude

observed immediately after the transition to standing. This response is immediate and, thus, not a regulatory response but, rather, a purely passive response that occurs because of the nature of the underlying fluid dynamics. We have described an elaborate model for predicting effects of hydrostatic changes, even though this model was only validated for the transition from sitting to standing, i.e., $\cos(\psi) = 1$. The advantage of the model derived in the present work is that it may be applicable to prediction of hydrostatic effects observed during tilt-table experiments.

The main accomplishment of this work is that our model describes how autonomic regulation and cerebral autoregulation play a synergistic role in the control of arterial blood pressure and cerebral blood flow velocity. In particular, the cerebral resistance first decreases and then increases during active standing. This result is different from previous findings (27), which suggested an initial increase followed by a decrease. However, the new result is not surprising, because the present study was performed with a more complex closed-loop model. The main advantage of the closed-loop 11-compartment model presented in this study is that the cerebrovascular resistance offers a more accurate representation of the brain. For example, in previous work (27), the measured pressure was an input and only one compartment was included. Hence, the peripheral resistance was not distinguished between resistance of the body and the brain. Furthermore, the curve for R_{acp} displays hysteresis effects: Immediately after standing, the decrease of R_{acp} is faster than the increase for $t \leq 70$ s during the phase where blood flow velocity is returning to its normal value. Hysteresis in vascular resistance in response to decreasing and increasing pressures may reflect differences between cerebral and peripheral vasculature that account for time lags between central and peripheral responses. With normal autoregulation, blood flow velocity precedes changes in peripheral blood pressure, reflecting local adjustments to intracranial pressure (26). Finally, to obtain a blood flow velocity during standing that is equivalent to that during sitting, the resistance reaches a set point that is higher during standing than during sitting.

Results for parameters representative of autonomic regulation show that these parameters react as expected: peripheral resistance and cardiac contractility increase, while compliance decreases (Fig. 10). As described in RESULTS, the contractility increases much faster than the peripheral resistance. This could be due to the more rapid effects of parasympathetic withdrawal acting on contractility than of sympathetic activation, which has a later effect on contractility, peripheral resistance, and compliance.

Finally, the optimized parameters depend on the initial estimates and the optimization algorithm. In particular, some of the maximum values for the resistances and compliances have large values, which are physiologically unrealistic.

APPENDIX

The complete system of differential equations needed to describe all flows and pressures shown in Fig. 1 consists of 11 ordinary differential equations. For each of the nine compartments that represent the arteries and veins, we obtain differential equations of the form of Eq. 2

$$C_a \frac{dp_a}{dt} = q_{av} - q_{ac} - q_{af} - q_{au} - p_a \frac{dC_a}{dt}$$

$$C_{au} \frac{dp_{au}}{dt} = q_a - q_{al} - q_{aup} - p_{au} \frac{dC_{au}}{dt}$$

$$C_{al} \frac{dp_{al}}{dt} = q_{au} - q_{alp} - p_{al} \frac{dC_{al}}{dt}$$

$$C_{af} \frac{dp_{af}}{dt} = q_a - q_{afp} - p_{af} \frac{dC_{af}}{dt}$$

$$C_{ac} \frac{dp_{ac}}{dt} = q_{ac} - q_{acp} - p_{ac} \frac{dC_{ac}}{dt}$$

$$C_{vl} \frac{dp_{vl}}{dt} = q_{alp} - q_{vl} - p_{vl} \frac{dC_{vl}}{dt}$$

$$C_{vu} \frac{dp_{vu}}{dt} = q_{vl} + q_{aup} - q_{vu} - p_{vu} \frac{dC_{vu}}{dt}$$

$$C_v \frac{dp_v}{dt} = q_{vu} + q_{afp} + q_{vc} - q_v - p_v \frac{dC_v}{dt}$$

$$C_{vc} \frac{dp_{vc}}{dt} = q_{acp} - q_{vc} - p_{vc} \frac{dC_{vc}}{dt}$$

where each of the flows is determined using Kirchoff's current law. The flows are as follows

$$q_{av} = \frac{p_{lv} - p_a}{R_{av}}$$

$$q_{au} = \frac{p_a - p_{au}}{R_{au}}$$

$$q_{al} = \frac{p_{au} - p_{al} - \rho gh}{R_{al}}$$

$$q_{af} = \frac{p_a - p_{af}}{R_{af}}$$

$$q_{ac} = \frac{p_a - p_{ac}}{R_{ac}}$$

$$q_{aup} = \frac{p_{au} - p_{vu}}{R_{aup}}$$

$$q_{alp} = \frac{p_{al} - p_{vl}}{R_{alp}}$$

$$q_{afp} = \frac{p_{af} - p_v}{R_{afp}}$$

$$q_{acp} = \frac{p_{ac} - p_{vc}}{R_{acp}}$$

$$q_v = \frac{p_v - p_{la}}{R_v}$$

$$q_{vu} = \frac{p_{vu} - p_v}{R_{vu}}$$

$$q_{vl} = \frac{p_{vl} - p_{vu} + \rho gh}{R_{vl}}$$

$$q_{vc} = \frac{p_{vc} - p_v}{R_{vc}}$$

$$q_{mv} = \frac{p_{la} - p_{lv}}{R_{mv}}$$

Finally, differential equations for the two compartments that represent the left atrium and ventricle are given by

$$\frac{dV_{lv}}{dt} = q_{mv} - q_{av}$$

$$\frac{dV_{la}}{dt} = q_v - q_{mv}$$

For these compartments, pressures are computed using the heart model (see MODELING BLOOD PRESSURE AND BLOOD FLOW VELOCITY. *Ventricular and atrial contraction*).

ACKNOWLEDGMENTS

This work was supported by US-Austria-Denmark Cooperative Research: Modeling and Control of the Cardiovascular-Respiratory System Grant 0437037 from the National Science Foundation. Work performed at Beth Israel Deaconess Medical Center General Clinical Research Center was supported by National Institutes of Health Grants M01 RR-01302, R01 NS-045745-01A2, and P60 AG-08812. L. Ellwein was supported by predoctoral National Research Service Award Training Grant TR32-AG-023480 and a Statistical and Applied Mathematical Sciences Institute graduate fellowship. Data collection and analysis were supported by a Joseph Paresky Men's Associates grant from the Hebrew Rehabilitation Center for Aged, National Institute on Aging Research Nursing Home Grant AG-04390, and Alzheimers Disease Research Center Grant AG-05134. H. Tran was supported in part by National Institute of General Medical Sciences Grant RO1 GM-067299-03.

REFERENCES

1. Aaslid R, Markwalder TM, and Nornes H. Noninvasive transcranial Doppler ultrasound recording of flow velocity in basal cerebral arteries. *J Neurosurg* 57: 769-774, 1982.
2. Aaslid R. Cerebral hemodynamics. In: *Transcranial Doppler*, edited by Newell DW and Aaslid R. New York: Raven, 1992, p. 49-55.
3. Beneken JEW and DeWit B. A physical approach to hemodynamic aspects of the human cardiovascular system. In: *Physical Basis of Circulatory Transport: Regulation and Exchange*, edited by Guyton AC and Reeve EB. Philadelphia, PA: Saunders, 1966, p. 1-45.
4. Bullock J, Boyle J, and Wang M. *Physiology* (4th ed.). Philadelphia, PA: Lippincott Williams & Wilkins, 2001.
5. Danielsen M. *Modeling of Feedback Mechanisms Which Control the Heart Function in a View to An Implementation in Cardiovascular Models* (PhD thesis). Roskilde, Denmark: Roskilde University, 1998.
6. Danielsen M and Ottesen JT. Describing the pumping heart as a pressure source. *J Theor Biol* 212: 71-81, 2001.
7. Guyton AC and Hall JE. *Textbook of Medical Physiology* (9th ed.). Philadelphia, PA: Saunders, 1996.
8. Heldt T, Shim EB, Kamm RD, and Mark RD. Computational modeling of cardiovascular response to orthostatic stress. *J Appl Physiol* 92: 1239-1254, 2002.
9. Kappel F and Peer RO. A mathematical model for fundamental regulation processes in the cardiovascular system. *J Math Biol* 31: 611-631, 1993.
10. Kappel F, Lafer A, and Peer RO. A model for the cardiovascular system under an ergometric workload. *Surv Math Ind* 7: 239-250, 1997.
11. Kappel F and Batzel JJ. Survey of research in modeling the human respiratory and cardiovascular systems. In: *Research Directions in Distributed Parameter Systems*, edited by Smith RC and Demetriou MA. Philadelphia, PA: SIAM, 2003, p. 187-218.
12. Kaufmann H. Syncope. A neurologist's viewpoint. *Cardiol Clin* 15: 177-194, 1997.
13. Kelley C. *Iterative Methods for Optimization*. Philadelphia, PA: SIAM, 1999.
14. Landau LD and Lifshitz EM. *Fluid Mechanics* (2nd ed.). Oxford, UK: Pergamon, 1993, p. 57.
15. Lipsitz LA, Mukai S, Hamner J, Gagnon M, and Babikian V. Dynamic regulation of middle cerebral artery blood flow velocity in aging and hypertension. *Stroke* 31: 1897-1903, 2000.

16. **Low PA.** Autonomic nervous system function. *J Clin Neurophysiol* 10: 14–27, 1993.
17. **Low PA and Bannister RG.** Multiple system atrophy and pure autonomic failure. In: *Clinical Autonomic Disorders*, edited by Low PA. Philadelphia, PA: Lippincott-Raven, 1997, p. 555–575.
18. **Low PA, Novak V, Spies JM, and Petty G.** Cerebrovascular regulation in the postural tachycardia syndrome (POTS). *Am J Med Sci* 317: 124–133, 1999.
19. **Melchior FM, Scrivinasen RS, and Charles JB.** Mathematical modeling of the human response to LBNP. *Physiologist* 35 Suppl 1: S204–S205, 1992.
20. **Melchior FM, Scrivinasen RS, and Clere JM.** Simulation of cardiovascular response to lower body negative pressure from 0 mmHg to –40 mmHg. *J Appl Physiol* 77: 630–640, 1994.
21. **Neumann S.** *Modeling Acute Hemorrhage in the Human Cardiovascular System* (PhD thesis). Philadelphia, PA: University of Pennsylvania, 1996.
22. **Njemanze PC.** Cerebral circulation dysfunction and hemodynamic abnormalities in syncope during upright tilt test. *Can J Cardiol* 9: 238–242, 1993.
23. **Noordergraaf A.** *Circulatory System Dynamics*. New York: Academic, 1978, p. 24.
24. **Novak V, Honos G, and Schondorf R.** Is the heart “empty” at syncope? *J Auton Nerv Syst* 60: 83–92, 1996.
25. **Novak V, Novak P, Spies JM, and Low PA.** The autoregulation of cerebral blood flow in orthostatic hypotension. *Stroke* 29: 104–111, 1998.
26. **Novak V, Yang ACC, Lepicovsky L, Goldbeger AL, Lipsitz LA, and Peng CK.** Multimodal pressure-flow method to assess dynamics of cerebral autoregulation in stroke and hypertension. *BioMed Eng Online* 3: 39, 2004.
27. **Olufsen MS, Nadim A, and Lipsitz LA.** Dynamics of cerebral blood flow regulation explained using a lumped parameter model. *Am J Physiol Regul Integr Comp Physiol* 282: R611–R622, 2002.
28. **Olufsen MS and Nadim A.** On deriving lumped models for blood flow and pressure in the systemic arteries. *Math Biosci Eng* 1: 61–80, 2004.
29. **Olufsen MS, Tran A, and Ottesen JT.** Modeling cerebral blood flow control during posture change from sitting to standing. *Cardiovasc Eng* 4: 47–58, 2004.
30. **Ono K, Uozumi T, Yoshimoto C, and Kenner T.** The optimal cardiovascular regulation of the arterial blood pressure. In: *Cardiovascular System Dynamics: Model and Measurements*, edited by Kenner T, Busse R, and Hinghofer-Szalkay H. New York: Plenum, 1982, p. 119–139.
31. **Ottesen JT.** Modeling of the baroreflex-feedback mechanism with time-delay. *J Math Biol* 36: 41–63, 1997.
32. **Ottesen JT.** Nonlinearity of baroreceptor nerves. *Surv Math Ind* 7: 187–201, 1997.
33. **Ottesen JT and Danielsen M.** Modeling ventricular contraction with heart rate changes. *J Theor Biol* 222: 337–346, 2003.
34. **Panerai RB.** Assessment of cerebral pressure autoregulation in humans—a review of measurement methods. *Physiol Meas* 19: 305–338, 1998.
35. **Rideout V.** *Mathematical and Computer Modeling of Physiological Systems*. Englewood Cliffs, NJ: Medical Physics Publishing, 1991.
36. **Serrador JM, Picot PA, Rutt BK, Shoemaker JK, and Bondar RL.** MRI measures of middle cerebral artery diameter in conscious humans during simulated orthostasis. *Stroke* 31: 1672–1678, 2000.
37. **Smith JJ and Kampine JT.** *Circulatory Physiology, the Essentials* (3rd ed.). Baltimore, MD: Williams & Wilkins, 1990.
38. **Tiecks FP, Lam AM, Aaslid R, and Newell DW.** Comparison of static and dynamic cerebral autoregulation measurements. *Stroke* 26: 1014–1019, 1995.
39. **Ursino M and Lodi CA.** Interaction among autoregulation, CO₂ reactivity, and intracranial pressure: a mathematical model. *Am J Physiol Heart Circ Physiol* 274: H1715–H1728, 1998.
40. **Ursino M.** Interaction between carotid baroregulation and the pulsating heart: a mathematical model. *Am J Physiol Heart Circ Physiol* 275: H1733–H1747, 1998.
41. **Warner HR.** The frequency-dependent nature of blood pressure regulation by carotid sinus studied with an electric analog. *Circ Res* 6: 35–40, 1958.
42. **Warner HR.** Use of analogue computers in the study of control mechanisms in the circulation. *Fed Proc* 21: 1962.
43. **Warner HR and Cox A.** A mathematical model of heart rate control by sympathetic and vagus efferent information. *J Appl Physiol* 17: 349–358, 1962.
44. **Wesseling KH, Stettels JJ, Walstra G, Van Esch HJ, and Donders JH.** Baromodulation as the cause of short-term blood pressure variability. In: *Application of Physics to Medicine and Biology*, edited by Alberi G, Bajzer Z, and Baxa P. Singapore: World Scientific, 1982, p. 247–276.